Pipetting Nanowires: In Situ Visualization of Solid-State Nanowire-to-Nanoparticle Transformation Driven by Surface Diffusion-Mediated Capillarity

Maria Eugenia Toimil-Molares, Lars Röntzsch, Wilfried Sigle, Karl-Heinz Heinig, Christina Trautmann, and Reinhard Neumann*

The most interesting applications of nanotubes include their use as storage media for atoms and small molecules, as nanoscale capsules for chemical reactions, and as nanopipettes for material delivery. The geometrical transformation of metallic copper nanowires, confined in graphitic coating, into crystalline nanoparticles of up to tenfold increased diameter is reported. In situ transmission electron microscopy images at 500 °C, recorded as movies, provide an exceptional real-time visualization of Cu draining out of the carbon coating. The solid content of the carbon tube is effectively evacuated over micrometer distances towards the open end, transforming each nanowire into a single monocrystalline, facetted Cu particle. Kinetic Monte Carlo simulations propose that this dramatic morphological transformation is driven by surface diffusion of Cu atoms along the wire/tube interface, thus minimizing the total free energy of the system.

1. Introduction

Capillarity is the basis for many biological, physical, and technological processes. Nanotubes with diameters of few to hundred nanometers are the smallest synthetic capillaries available nowadays and are thus ideal materials to study capillary forces at the nanoscale.[1] Foreseeable applications for nanotubes include storage or encapsulation of atoms or small molecules and catalysts for chemical reactions.[2] Reversible wetting and filling of single-wall carbon nanotubes (CNTs) with mercury droplets by electrocapillary pressure was already demonstrated.[3] Recent theoretical studies suggest that CNTs can act as nanocapillaries absorbing or withdrawing non-wetting, liquid silver droplets.[4,5] In the case of encapsulated solid material, capillary processes can be triggered by enhancing diffusion processes at elevated temperatures. Metal migration processes in nanoparticle/carbon tube heterostructures have been utilized to reversibly deliver metal clusters at predetermined positions.[6–8] Recently, Moseler et al. visualized the restructuring of few nanometer diameter solid nickel catalyst nanoparticles during carbon nanotube growth by environmental transmission electron microscopy (TEM).[9] They successfully modelled the process using molecular dynamics, finding that capillary-driven surface diffusion is the dominant transport mechanism. Additionally, the withdrawal of a 10 nm solid silver nanoparticle from a CNT tip in the presence of an external Ag nanoparticle has been reported recently.[10] The improved understanding of both filling and draining processes driven by capillary action at the nanoscale is highly important for applications in nanoelectronics, biology, and medicine.[11–15]

This report visualizes the solid-state morphological transformation of several micrometer long carbon-coated Cu nanowires into single-crystalline Cu nanoparticles. The process is observed at 500 °C, significantly below the melting temperature, and is driven by surface-diffusion mediated capillarity. By in situ TEM the mass transport of Cu along the interfacial layer between wire and carbon sheath was followed in real time. The images represent a direct visualization how the surface free-energy yields minimization at the nanoscale. While the tube is slowly and continuously drained at one end, a facetted Cu particle is growing at the other end. Within about one hour, the transformation of the encapsulated nanowire into a single-crystalline facetted Cu nanoparticle is completed. In situ high-temperature TEM allowed us to record this dramatic geometrical change continuously and unveils pronounced solid-state mass transport at the nanoscale. Kinetic Monte Carlo (KMC) simulations suggest that the process is driven by surface diffusion of Cu atoms along the wire/tube interface, thus, minimizing the total surface free energy of the system. The results demonstrate that by controlling the atomic diffusion processes of metals within nanotube recipients, the metal forming micrometer-long nanostructures can be delivered to predetermined positions with mass and rate control.

Dr. M. E. Toimil-Molares, Prof. C. Trautmann, Prof. R. Neumann
GSI Helmholtz Centre for Heavy Ion Research
Planckstr. 1, 64291 Darmstadt, Germany
E-mail: M.E.ToimilMolares@gsi.de
Dr. L. Röntzsch, Dr. K.-H. Heinig
Helmholtz-Centre Dresden-Rossendorf
Postbox 510119, 01314 Dresden, Germany
Dr. L. Röntzsch
Fraunhofer Institute IFAM
Winterbergstr. 28, 01277 Dresden, Germany
Dr. W. Sigle
Max-Planck Institute for Metal Research
70569 Stuttgart, Germany

DOI: 10.1002/adfm.201102260

2. Results

The low-magnification TEM image in **Figure 1**a displays two encapsulated copper nanowires (diameter ≈ 30 nm) intersecting each other on a TEM grid. For better identification, labels are assigned to the wire ends, i.e., the horizontal wire extends from 1 to 2 and the vertical wire from 3 to 4. The TEM images in Figure 1b,c depict the respective ends, 1 and 4, after 8 min of annealing at 500 °C. The tube surrounding the nanowire is indicated by arrows in both figures. The high-resolution image displayed in Figure 1d gives evidence that the tube consists of a multishell graphitic coating that is resistant throughout the whole process. The layer is presumably formed from polymer residues on the nanowire surface remains from the synthesis process. The formation of similar nanotube/nanoparticle heterostructures has been reported previously. For example, Helveg et al. reported the synthesis of carbon nanofibers from methane decomposition over Ni nanocrystals.[16] Also Sutter et al. demonstrated that temperatures higher than 425 °C in combination with electron beam exposure drive the formation of Au/C core/shell nanoparticles.[17] Formation of CNT/nanowire heterostructures was also observed during the synthesis of Si/Ge nanowires in the TEM at high temperatures by liquid vapor deposition,[18] and on GaN wires when small indium metal clusters are introduced on the wire surface.[19]

The fact that the carbon tubes around the Cu wires provide drainage at their open ends and that the rest of the remaining wire is crystalline and without any morphology change is the first strong indication of Cu mass transport by diffusion. **Figure 2** displays a series of snapshots taken at different times and at four fixed positions between wire ends 1 and 2 (respective color-boxes areas are followed in panels (b–e) in Figure 2a). The corresponding videos are included in the Supporting Information S1–S4. Unexpected but obvious from the consecutive images in the video, the velocity of the Cu edge increases with time and location during the annealing process although the temperature was kept constant. The first set of images was recorded after 44 min annealing (Figure 2b and Supporting Information Video S1), showing the slow motion of the wire edge towards the right at an effective longitudinal velocity of 2.1 nm s^{-1} (103 nm within 50 s). After 55 min annealing (Figure 2c and Supporting Information Video S2), the wire edge moves across the intersection region. The velocity during this stage is 1.8 nm s^{-1}, i.e., slightly slower, probably due to the underlying nanowire/nanotube. After 61 min annealing (Figure 2d and Supporting Information Video S3), the velocity of the moving copper has increased to 4.8 nm s^{-1}, and finally in the last image series (Figure 2e and Supporting Information Video S4), the process is further accelerated to 14.8 nm s^{-1} (108 nm within 8 s). When approaching end 2 of the wire/tube, the displacement of the wire edge is seven times faster than at the initial stage close to end 1. In particular the consecutive images of the video give clear evidence that the morphology of the wire edge remains faceted and an almost layer-by-layer atomic movement occurs during the process.

These snapshots and the videos display the important fact of this experiment that the morphology of the Cu front

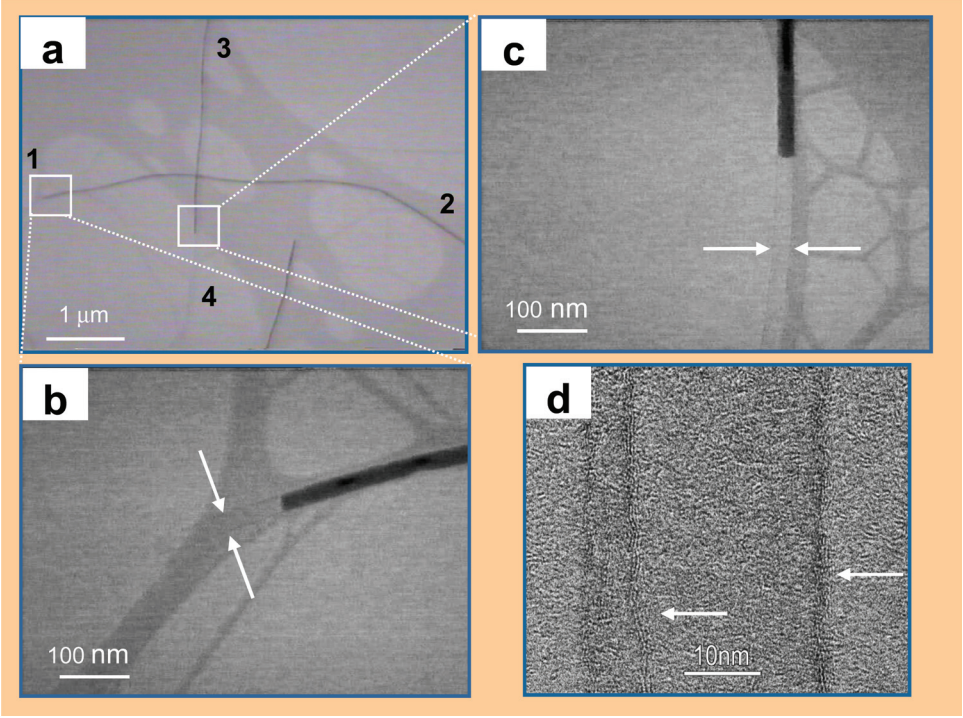

Figure 1. a) TEM image of two crossing Cu nanowires on a TEM grid during annealing at a temperature $T = 500$ °C. Horizontal and vertical wires are denoted 1,2 and 3,4, respectively. The image in (a) was recorded after annealing for 7 min. b,c) Higher magnification of the marked insets showing wire endings 1 and 4. The arrows indicate the few nanometer thick carbon coatings formed around the metal nanowires. d) High-resolution TEM image of the carbon coating displaying the graphitic layers.

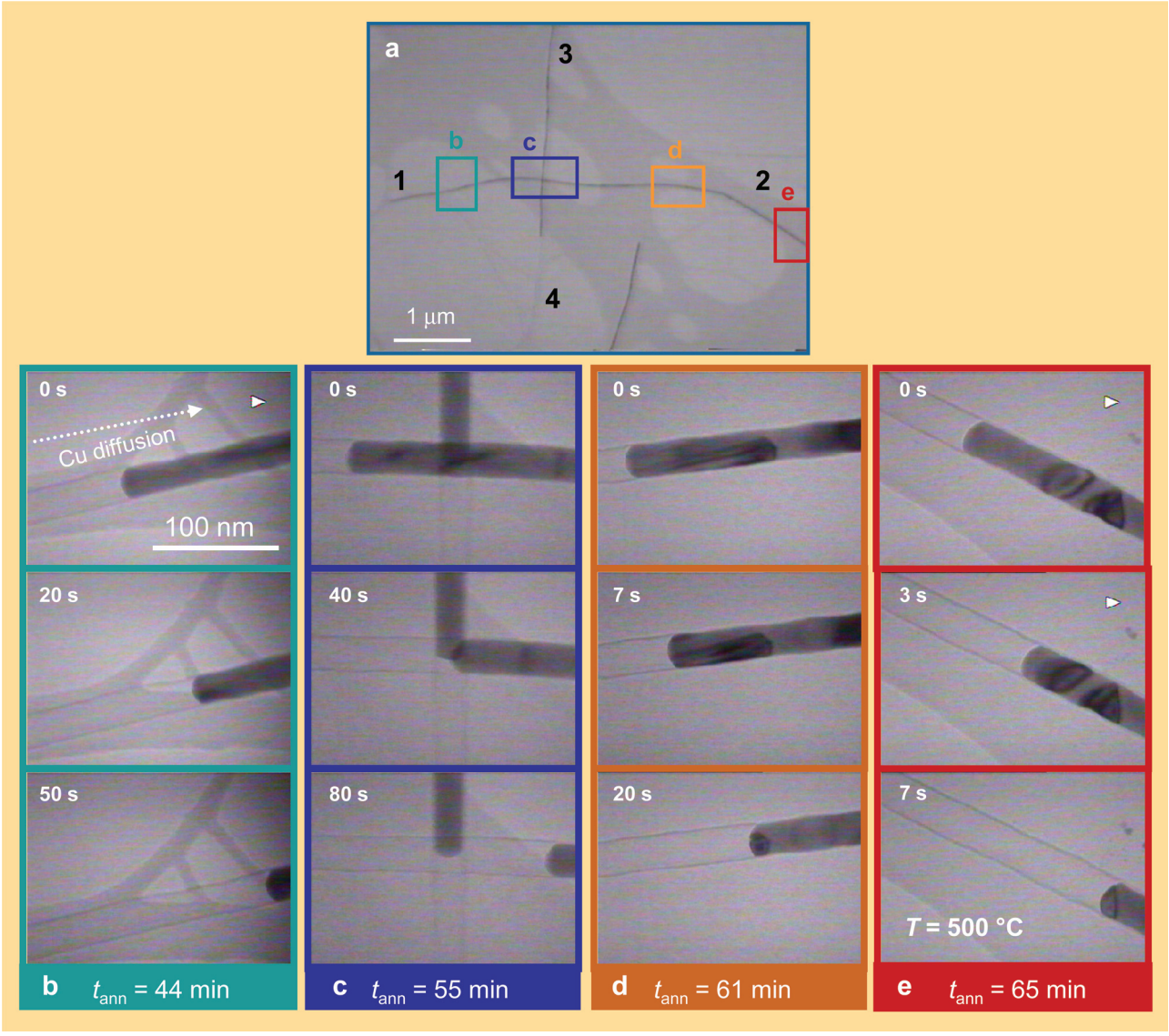

Figure 2. Snapshots of the video recorded on four areas indicated in a) at different annealing times: b) 44, c) 55, d) 61, and e) 65 min. In each case, the time series (from top to bottom) shows that the Cu filling moves from left to right, while the carbon shell remains unchanged. For all snapshot images the scale bar is 100 nm.

remains faceted and diffraction contrasts along the Cu wire originating from planar defects such as twin or grain boundaries are visible (in particular in Figure 2d,e). During the dynamic process, the planar defects remain stable while the crystal continuously recedes from left to right across the defect zone. These observations clearly exclude melting and verify that the nanowire is fully in the solid phase. In fact, at 500 °C melting of our Cu nanowires can be excluded since the melting point of bulk copper is 1058 °C and a decrease of the melting temperature due to size effects is not expected as long as the size of the Cu nanostructure is larger than 5 nm.[20,21] Thus, morphological changes are attributed to atomic diffusion of Cu atoms taking place at 500 °C. This complements previous works that report instabilities of Ge nanowires attributed to surface and volume melting[18] and on Co nanowires attributed to sublimation.[22]

Mass conservation raises the question: Where is the Cu moving to and what is the driving force? Complementing the observation in Figure 2, we also recorded the events occurring at the open end of the tubes. The sequence of TEM images displayed in **Figure 3**a–d was taken after 9, 50, 65, and 75 min annealing at 500 °C and evidences a dramatic morphological change. About 300 nm before the end 2 of the wire (probably at a defective aperture of the carbon tube), a protrusion starts to form with larger dimensions than the initial nanowire diameter. The size of the protrusion increases progressively as Cu diffuses first predominantly from the left side and finally also from the right-sided tube delivering more and more material. During the annealing process, the enlarging particle presents facets, again indicating that the process takes place in the solid state. After approximately 70 min, every Cu nanowire on the TEM grid had undergone a morphological transformation into

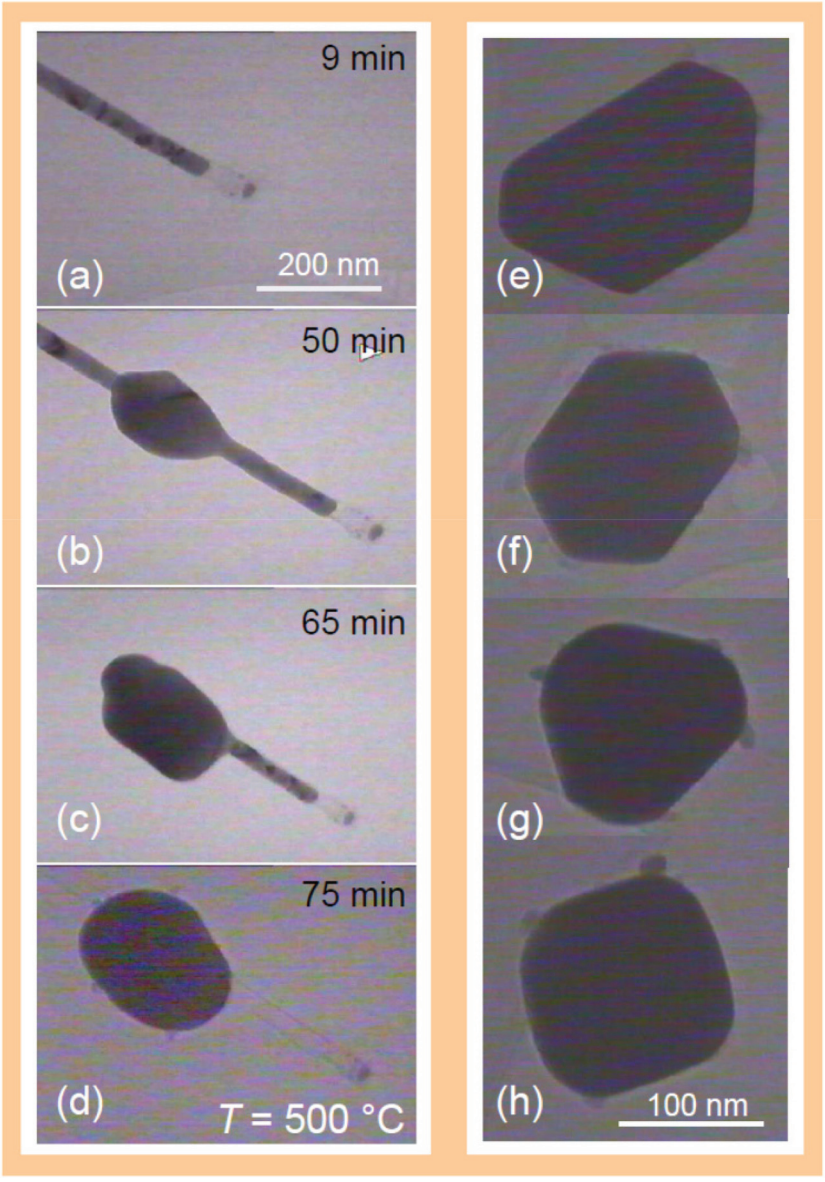

Figure 3. a–d) TEM images of Cu nanowire close to end 2 (cf. Figure 1) recording the formation and growth of a nanoparticle at different times of the annealing process. e–h) Facetted Cu particles observed at different wire ends after 80 min annealing.

a facetted nanoparticle (Figure 3e–h). The different geometries represent projections of the equilibrium shape of faced-centered cubic (fcc) Cu crystals,[23] the rounded corners being ascribed to the elevated temperature.

The transformation process under annealing is significantly different from morphological shape changes observed for non-embedded Cu and Au nanowires that fragment and convert into chains of nanospheres. This latter process is driven by the Rayleigh instability,[24–26] where the size of the nanospheres is expected to be around twice the size of the initial wire diameter. In the experiment reported here, a pea-pod-like arrangement is not possible because the carbon tube tightly confines the metallic filling preventing radial undulations of the Cu nanowire as required by the Rayleigh instability criterion. The alternative to minimize the surface free energy is the direct transformation into a single particle at an open end of the confining tube or at any other location where the tube has an opening. Although details of the solid-state draining mechanism are not completely understood, we suggest capillary forces drive the withdrawal of Cu from several micrometers long nanoscale carbon tubes into small facetted Cu crystals.

Three-dimensional lattice KMC simulations yield qualitatively a very similar behavior and indicate that surface diffusion is responsible for the draining of the metal filled tube. The KMC method describes the process entirely on the atomistic level and was previously used successfully to explain various diffusion-controlled morphological changes of metal and semiconductor nanostructures in the solid state.[27–30] Details on the KMC method are given in ref. [31]. Here, discrete diffusion jumps of atoms based on Ising-type nearest-neighbor (NN) pair interactions J_{NN} are considered on a fcc lattice. A system size of 128 × 128 × 256 lattice sites was used (a = lattice parameter, NN distance = $\sqrt{2}a$). The kinetics is described by transitions of configurational states (single diffusion events), which cause a change of the internal energy (ΔE) of the system. These state transitions are thermally activated and occur with a defined Boltzmann-like probability $P \propto \exp[-\Delta E/(k_B T)]$, where k_B and T denote the Boltzmann constant and the absolute temperature, respectively, at a certain attempt frequency, thereby defining a linear time scale, which is measured in Monte Carlo steps (MCS).[31] The state transition probability according Metropolis et al. was applied.[32] The series of states the system is running through is called the "reaction pathway". Starting from a non-equilibrium state, it reflects the system's free evolution (relaxation) in an approximate manner. Although based on simplified atomistic dynamics, the approach allows studying the spatiotemporal development of systems containing up to several ten thousand atoms for time spans over several orders of magnitude. **Figure 4** presents a series of snapshots where 28 847 atoms (with pair interaction $J_{NN}/(k_B T) = 1.5$) are confined in a cylindrical tube that is closed on one side and open at the other end (tube radius = 10a; tube length = 180a). It is assumed that there is no attractive interaction between the filling material and the tube. This is a good approximation for the very weak pairwise binding energy between graphite and fcc metals such as Cu or Ag compared to the pairwise binding energy of the respective metal atoms.[5,33] During the first stage, the filling material swells out at the open end forming a protrusion that gradually turns into a spherical crystal. As evolution proceeds, the entire

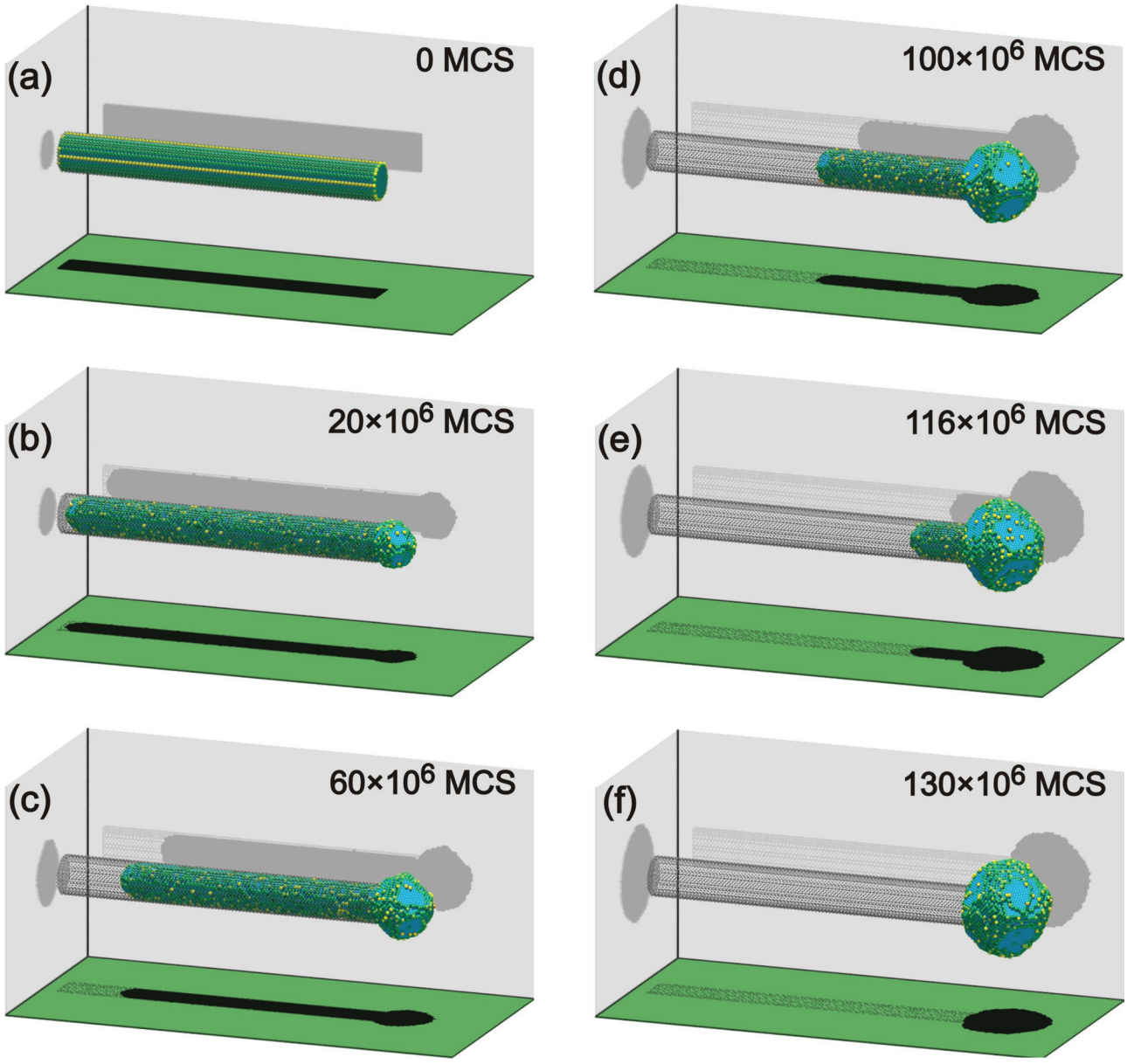

Figure 4. Snapshots from kinetic Monte Carlo simulations showing the reaction pathway of the draining process of a metal filled tube with an open end. The time is indicated in number of MCS. The color of the atoms indicates the energetic state expressed as number of nearest neighbors (e.g., 3 NNs in yellow; 9 NNs in blue).

material diffuses out of the tube and a single crystal with (111) facets is formed. In fcc materials the (111) facet is known to have the lowest surface free energy.[34] Finally, the tube is empty and all material is accumulated in the nanocrystal formed at the open end of the tube.

In view of solid-state capillarity, the draining process can be described as follows: In the initial stage, the curvature of the inner nanowire edge $1/R_t$ is larger than that of the protrusion $1/R_c$ (here, R_t and R_c denote the inner radius of the tube and the radius of the protruding particle; cf. inset in **Figure 5**). According to the Gibbs–Thomson equation, this results in a gradient of chemical potential (ad-atom concentration) from the inside to the outside that in turn drives a diffusive flux of ad-atoms towards the open end. This diffusive flux shortens the length of the remaining filling $l(t)$ inside the tube because of mass conservation. Over the whole process, the curvature of the wire front in the tube remains constant whereas the curvature of the protrusion decreases. The difference between the wire edge in the tube and the protruding particle steadily increases, thus enhancing the diffusive flux of ad-atoms towards the open end until all Cu atoms are accumulated in the particle (Figure 5). This effect is in excellent agreement with our TEM observations and explains the acceleration of the particle growth rate as annealing proceeds (Figure 2 and Supporting Information Videos S1–S4).

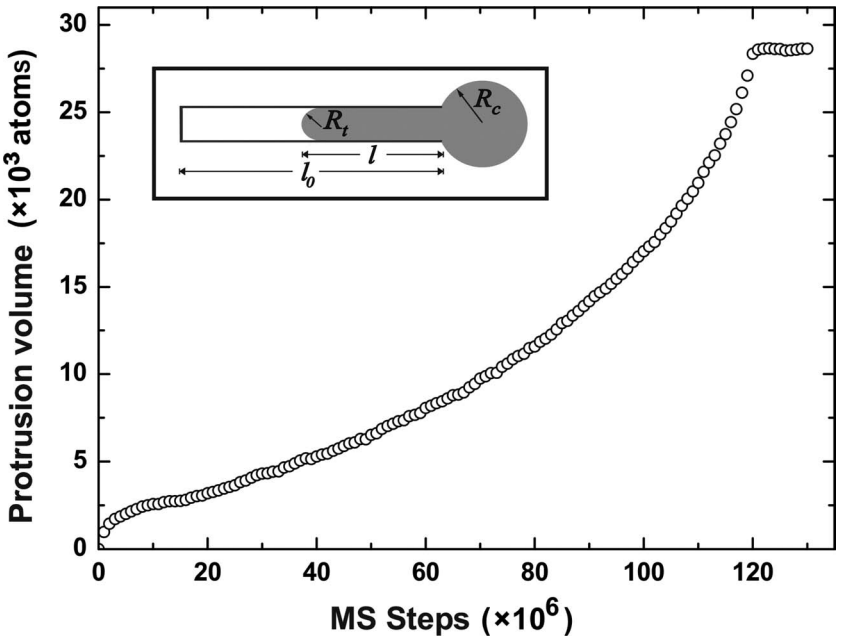

Figure 5. Time dependence of the protrusion volume. According to the 3D lattice KMC simulation shown in Figure 4, the time dependence displayed in MCS gives evidence that the diffusion-based protrusion growth is an accelerated process.

3. Conclusions

In summary, micrometer long Cu nanowires consisting of long single-crystalline sections, encapsulated by a solid, stable graphitic carbon layer, undergo a solid-state morphological transformation into larger facetted Cu nanoparticles at 500 °C. Real-time imaging by in situ electron microscopy provides evidence that the mass transport process occurs in the solid state excluding melting. Kinetic MC simulations ascribe the effect to capillarity-induced diffusion of Cu atoms along the interfacial layer between the solid wire and the carbon tube, driven by minimizing the total free energy of the system. The process shows that nanowires coated by electron-beam induced carbon tubes can serve as well defined nanopipettes. The extraction process is initiated and controlled by temperature. The template-based electrochemical wire synthesis allows control on wire diameter as well as length and thus provides material for nanocrystals whose size is predefined by the pipette volume.

4. Experimental Section

Cu nanowires were fabricated by electrochemical deposition in porous 30-μm-thick ion track-etched polymer membranes.[35,36] The polycarbonate (Makrofol N, Bayer) membranes were prepared by irradiation with GeV heavy ions at the UNILAC accelerator of GSI Helmholtz Centre (Darmstadt) and subsequent chemical etching of the ion tracks in a NaOH solution (6 N) at 50 °C. A thin gold film was sputtered onto one side of the membrane and reinforced electrochemically with copper to obtain a stable substrate, which served later as the cathode in the galvanic cell. The electrodeposition was performed potentiostatically at 50 °C using a solution of Cu_2SO_4 (240 g L^{-1}) and H_2SO_4 (20 g L^{-1}) as electrolyte. Nanowires fabricated under these conditions consist of long single-crystalline sections, oriented along the [110] direction.[35] After wire deposition, the polymer matrix was dissolved in dichloromethane. Although carefully rinsed, high-resolution scanning or transmission electron microscopy revealed polymer residues on the nanowire surface providing source material for carbonization and carbon tube formation in the electron beam. For TEM investigation, the wires were detached from the supporting Cu layer by sonication. During this procedure the wires break into sections of lengths between a few μm and 30 μm (initial length).[37] In a next step, some drops of the dichloromethane solution containing individual wires were dispersed on a conventional carbon-coated TEM grid and mounted on a variable-temperature sample holder. All TEM experiments were carried out in a JEOL JEM2000FX microscope using a high-temperature specimen holder operated in vacuum (10^{-6} mbar) at 500 °C (heating rate 100 K min^{-1}). Because of the long-term heating, the carbon thin film and the Cu wires were expected to be thermally equilibrated. The uncertainty of the sample temperature was assumed to be ±10 K. At such elevated temperatures, the presence of carbon (presumably from polymer residues on the wire surface) resulted in the formation of graphene layers entirely coating the nanowires. In every experiment, tens of wires were selected, their locations registered, and their morphology and structure investigated at different times as the annealing proceeded. The images were recorded on a video tape.

Supporting Information

Supporting Information is available from the Wiley Online Library or from the author. It includes four movies corresponding to the observations on areas A, B, C, and D, from which selected snapshots are depicted in Figure 2b–e.

Acknowledgements

The authors are grateful for discussions with S. Karim and T.W. Cornelius. They thank B. Zielbauer for technical support with data editing and Dr. G. Miehe for TEM imaging of carbon shell displaying the graphitic layers (Figure 1b).

Received: September 22, 2011
Revised: November 4, 2011
Published online: December 19, 2011

[1] S. C. Tsang, Y. K. Chen, P. J. F. Harris, M. L. H. Green, *Nature* **2004**, *372*, 159.
[2] A. Bianco, K. Kostarelos, M. Prato, *Curr. Opin. Chem. Biol.* **2005**, *9*, 674.
[3] J. Y. Chen, A. Kutana, C. P. Collier, K. P. Giapis, *Science* **2005**, *310*, 1480.
[4] D. Schebarchov, S. C. Hendy, *Nano Lett.* **2008**, *8*, 2253.
[5] D. Schebarchov, S. C. Hendy, *Nanoscale* **2011**, *3*, 134.
[6] B. C. Regan, S. Aloni, R. O. Ritchie, U. Dahmen, A. Zettl, *Nature* **2004**, *428*, 924.
[7] G. E. Begtrup, W. Gannett, T. D. Yuzvinsky, V. H. Crespi, A. Zettl, *Nano Lett.* **2009**, *9*, 1835.
[8] K. Kim, K. Jensen, A. Zettl, *Nano Lett.* **2009**, *9*, 3209.
[9] M. Moseler, F. Cervantes-Sodi, S. Hofmann, G. Csanyi, A. C. Ferrari, *ACS Nano* **2010**, *4*, 7587.

[10] K. Edgar, S. C. Hendy, D. Schebarchov, R. D. Tilley, *Small* **2011**, *7*, 737.
[11] M. Löffler, U. Weissker, T. Mühl, T. Gemming, J. Eckert, B. Büchner, *Adv. Mater.* **2011**, *23*, 541.
[12] S. H. Kim, W. I. Choi, G. Kim, Y. J. Song, G.-H. Jeong, R. Hatakeyama, J. Ihm, Y. Kuk, *Phys. Rev. Lett.* **2007**, *99*, 256407.
[13] A. Taylor, K. Lipert, K. Kramer, S. Hampel, S. Fussel, A. Meye, R. Klingeler, M. Ritschel, A. Leonhardt, B. Buchner, M. P. Wirth. *J. Nanosci. Nanotechnol.* **2009**, *9*, 5709.
[14] S. S. Wong, E. Joselevich, A. T. Woolley, C. L. Cheung, C. M. Lieber, *Nature* **1998**, *394*, 52.
[15] X. Fan, J. E. Barclay, W. Peng, Y. Li, X. Li, G. Zhang, D. J. Evans, F. Zhang, *Nanotechnology* **2008**, *19*, 165702.
[16] S. Helveg, C. López-Cartes, J. Sehested, P. L. Hansen, B. S. Clausen, J. R. Rostrup-Nielsen, F. Abild-Pedersen, J. K. Nørskov, *Nature* **2004**, *427*, 426.
[17] E. Sutter, P. Sutter, Y. Zhu, *Nano Lett.* **2005**, *5*, 2092.
[18] Y. Wu, P. Yang, *Appl. Phys. Lett.* **2000**, *77*, 43.
[19] E. Sutter, P. Sutter, R. Calarco, T. Stoica, R. Meijers, *Appl. Phys. Lett.* **2007**, *90*, 093118.
[20] S. L. Lai, J. Y. Guo, V. Petrova, G. Ramanath, L. H. Allen, *Phys. Rev. Lett.* **1996**, *77*, 99.
[21] Ph. Buffat, J.-P. Borel, *Phys. Rev. A* **1976**, *13*, 2287.
[22] D. Ciuculescu, F. Dumestre, M. Comesana-Hermo, B. Chaudret, M. Spasova, M. Farle, C. Amiens, *Chem. Mater.* **2009**, *21*, 3987.
[23] C. Jayaprakash, W. F. Saam, *Phys. Rev. B* **1984**, *30*, 3916.
[24] M. E. Toimil-Molares, A. G. Balogh, T. W. Cornelius, R. Neumann, C. Trautmann, *Appl. Phys. Lett.* **2004**, *85*, 5337.
[25] S. Karim, M. E. Toimil-Molares A. G. Balogh, W. Ensinger, T. W. Cornelius, E. U. Khan, R. Neumann, *Nanotechnology* **2008**, *17*, 5954.
[26] S. Karim, M. E. Toimil-Molares, A. G. Balogh, W. Ensinger, T. W. Cornelius, E. U. Khan, R. Neumann, *J. Appl. Phys. D* **2007**, *40*, 3767.
[27] L. Röntzsch, K.-H. Heinig, J. A. Schuller, M. L. Brongersma, *Appl. Phys. Lett.* **2007**, *90*, 044105.
[28] L. Röntzsch, K.-H. Heinig, B. Schmidt, A. Mücklich, W. Möller, J. Thomas, T. Gemming, *Phys. Status Solidi A* **2005**, *202*, R170.
[29] K.-H. Heinig, T. Müller, B. Schmidt, M. Strobel, W. Möller, *Appl. Phys. A* **2003**, *77*, 17.
[30] T. Müller, K.-H. Heinig, W. Möller, *Appl. Phys. Lett.* **2002**, *81*, 3049.
[31] M. Strobel, K.-H. Heinig, W. Möller, *Phys. Rev. B* **2001**, *64*, 245422.
[32] N. Metropolis, A. W. Rosenbluth, M. N. Rosenbluth, A. H. Teller, E. Teller, *J. Chem. Phys.* **1953**, *21*, 1087.
[33] S. M. Foiles, M. I. Baskes, M. S. Daw, *Phys. Rev. B* **1986**, *33*, 7983.
[34] C. Rottman, M. Wortis, *Phys. Rev. B* **1984**, *29*, 328.
[35] M. E. Toimil-Molares, V. Buschmann, D. Dobrev, R. Neumann, R. Scholz, I. U. Schuchert, J. Vetter, *Adv. Mater.* **2001**, *62*, 13.
[36] M. E. Toimil Molares, J. Broetz, V. Buschmann, D. Dobrev, R. Neumann, R. Scholz, I. U. Schuchert, C. Trautmann, J. Vetter, *Nucl. Instrum. Methods Phys. Res. B* **2001**, *185*, 192.
[37] M. E. Toimil-Molares, E. M. Höhberger, Ch. Schaeflein, R. H. Blick, R. Neumann, C. Trautmann, *Appl. Phys. Lett.* **2003**, *82*, 31.